Available online at www.sciencedirect.com
ScienceDirect
Polymer 48 (2007) 4691–4703
polymer
www.elsevier.com/locate/polymer

Aqueous dispersion of novel silylated (polyurethane-acrylic hybrid/clay) nanocomposite

Sankaraiah Subramani, Sung-Wook Choi, Jun-Young Lee, Jung Hyun Kim*

Nanosphere Process and Technology Laboratory, Department of Chemical Engineering and Biotechnology, Yonsei University, 134 Shinchon-Dong, Sudaemoon-Ku, Seoul-120-749, Republic of Korea

Received 27 March 2007; received in revised form 12 June 2007; accepted 13 June 2007
Available online 16 June 2007

Abstract

Organofunctional silane-modified clay was synthesized using an ion exchange technique. The evolution of the ion exchanged or grafted amount and of the yield were monitored as a function of the initial silane concentration by thermogravimetric analysis. Qualitative evidence of the presence of chemically attached silane molecules on clay was proved by Fourier transform infrared spectroscopy. The grafted amount determined by thermogravimetric analysis was in good agreement with the cation exchange capacity of pristine clay, as determined by confirming that the silanes, which replaced the sodium ions, are grafted onto the clay edges. Using the silane-modified clay, novel aqueous silylated (polyurethane-acrylic/clay) nanocomposite dispersions (SPUA – silylated polyurethane-acrylic) were prepared and studied. X-ray diffraction and transmission electron microscopy examinations indicate that the clay platelets are mostly intercalated or partially exfoliated in the SPUA matrix with a *d*-spacing of ~2–2.50 nm. SPUA/clay dispersion with higher clay content exhibits a marginal increase in the average particle size, however, silane-modified clay has a pronounced effect. In addition, the incorporation of clay can also enhance the thermal resistance and mechanical properties of SPUAs dramatically through the reinforcing effect of organophilic clay. Clay does not influence the location and peak broadness of the glass transition temperature (T_g) of the soft segment as well as hard segment domains in the SPUA/clay films. However, the T_g of hard segment domains of *N*-(2-aminoethyl)-3-aminopropyltrimethoxysilane (AEAPTMS)-clay nanocomposites were higher than those of commercial clay-based nanocomposites. Better water and xylene resistance of the silane-modified clay nanocomposites proved that trifunctional organosilane can be used as effective modifiers for clays. This method provides an efficient way to incorporate silane-modified clay in the SPUA matrix.

Keywords: Aqueous; Silylated polyurethane; Modification

1. Introduction

During the past several years, nanocomposite materials have attracted significant attention because the intimate combination of organic and inorganic components at the nanoscale offers prospects of new and synergistic properties. Nanoparticles often strongly influence the properties of composites at very low-volume fractions. This is mainly due to the small distance between particles and the conversion of large fractions of the polymer matrix near their surfaces into an interphase with different properties, as well as the consequent change in morphology. The geometrical shape of the particles plays an important role in determining the properties of the composites [1]. In general, the key step in the synthesis of these materials is the establishment of a chemical link between originally non-mixing phases. Although the interaction between the organic polymers and the inorganic surfaces has long been a common operation, a major need for new bonding techniques arose when glass fibers were first used as reinforcing agents in organic resins. Organosilanes are known as the best surface treating agents for hydrophilic silicas and many other types of substrates. Organically modified alkoxysilanes

* Corresponding author. Tel.: +82 2 2123 7633; fax: +82 2 312 0305.
E-mail address: jayhkim@yonsei.ac.kr (J.H. Kim).

0032-3861/$ - see front matter © 2007 Elsevier Ltd. All rights reserved.
doi:10.1016/j.polymer.2007.06.023

with the general formula $R_nSi(X)_{4-n}$, where X is a hydrolysable group and R is a functional terminal group, are particularly well suited for this purpose, and are often used to provide covalent bonding between inorganic fillers and polymer matrices, enhance interfacial adhesion and improve the mechanical properties of composite materials [2–4].

Recently, montmorillonite (MMT), a layered silicate with lamellar shape, has attracted intensive research interest for the preparation of polymer/clay nanocomposites. This is because the lamellar platelets of MMT display high in-plane strength, stiffness, and high aspect ratio [5]. Typically, the chemical structure of MMT consists of two fused silica tetrahedral sheets sandwiching an edge-shared octahedral sheet of either magnesium or aluminum hydroxide. The Na^+ and Ca^{2+} residing in the interlayer galleries can be replaced by organic cations such as alkylammonium ions, via a cationic-exchange reaction to render the hydrophilic layered silicate organophilic. There are two ways to modify the layered silicates, covalent bond formation on the edges and ion exchange with organic cations. Generally, long chain organoalkylammonium modified organophilic clays are used to make polymer/clay nanocomposites [6–8], but there are few reports which describe about the clay modified by organosilanes. These reports describe the silylation of clays by organochlorosilane through covalent bond formation [9–11]. Organoclays modified by a small amount of hexamethyldisilazane was reported to retard the intercalation of a polar polymer significantly, such as poly(styrene-*co*-acrylonitrile), into the clay gallery [12]. Herrera described mono- and trifunctionalsilane grafted laponite clay platelets in water-based polymer/clay nanocomposites [13].

Polyurethanes (PU) are functional polymers whose properties can be tailor-made by simply adjusting the compositions to meet the highly diversified demands of modern technology such as coatings, adhesives, reaction injection molding, fibers, foams, rubbers, thermoplastic elastomers, and composites [14]. Conventional polyurethane products such as coatings and adhesives contain a significant amount of organic solvents and highly reactive isocyanate monomers. As waterborne polymer systems are environmentally friendly, the solvent-based polyurethanes have been gradually replaced by waterborne polyurethanes in the recent years and widely used in coatings and adhesive industries. For better performance of water and solvent-based polyurethane, they are modified either by varying polyurethane microstructures or by dispersing inorganic fillers, especially by incorporating nanosized layered silicates within the polyurethane continuous matrix.

There are many papers in the literature about solvent-based PU/clay nanocomposites and these research papers have described the effect of incorporation of nanolayers of mineral clay on the thermal stability [15–17], mechanical strength [18–20], morphology and elasticity [8] properties of these nanocomposites. Only a few waterborne polyurethane/clay nanocomposites have been reported in the literature, which were prepared by a prepolymer mixing process [6,7,21,22]. To our best knowledge, there is no information presented about the study of aminoalkyl trifunctional silane-modified clay and waterborne isocyanate free SPUA and SPUA/clay nanocomposites. The main objectives of this work were the synthesis of trifunctional silane-modified clay and the study of modified clay by XRD, FT-IR and TGA and to study the morphology, physical properties, glass transition, and mechanical properties of the modified clay reinforced SPUA/clay nanocomposites.

2. Experimental

2.1. Materials

Poly(tetramethylene glycol) (PTMG, molecular weight = 2000 g/mol, OH functionality = 2.0, Dongsung Chemical, Korea) and 1,4-butane diol (BD, Yakuri Pure Chemicals Co., Ltd, Japan) were dried in a vacuum at 80 °C for 12 h before use. Dimethylol propionic acid (DMPA, Aldrich, USA) was dried at 50 °C for 24 h in a vacuum oven. *N*-Methyl-2-pyrrolidone (NMP, Lancaster, UK) and acetone were stored in well-dried molecular sieves. Isophorone diisocyanate (IPDI, Aldrich, USA), triethylamine (TEA, Duksan Pharmaceutical Co., Ltd, Korea) and [3-(phenylamino)propyl]trimethoxysilane (PAPTMS, Aldrich, USA) were used as received. The monomers, methylmethacrylate (MMA, Junsei Chemicals Co., Ltd, Japan) and methacryloxypropyltrimethoxysilane (MAPTMS, Aldrich, USA) were used as received. The initiator, potassium persulphate (KPS, Duksan Pure Chemicals Co., Ltd, Korea) was recrystallized before use. A natural sodium montmorillonite clay, Cloisite Na^+ (Southern Clay Product Inc., USA), with a cation exchange capacity (CEC) of 92.6 mequiv/100 g was dried at 80 °C for 24 h under vacuum conditions. An organophilic clay, Cloisite 10A, specific gravity of 1.90 g/cc (Southern Clay Product Inc., USA) was dried at 80 °C for 24 h under vacuum conditions. The cations of natural montmorillonite in this organophilic clay were replaced by dimethyl, benzyl and hydrogenated tallow quaternary ammonium ions. The weight loss at ignition is 39% and the modifier concentration of clay is 125 mequiv/100 g of clay. The organic (surface) modifier, *N*-(2-aminoethyl)-3-aminopropyltrimethoxysilane (AEAPTMS, Aldrich, USA) was used as received. The catalyst, di-butyl tin dilaurate (DBTDL, Aldrich, USA) was used as received. Aqueous dispersions were prepared using Milli-Q water of 18 MΩ.

2.2. Preparation of inorganic-organophilic clay

Pristine hydrophilic clay was modified with intercalant using cation-exchange technique to increase the compatibility or interaction for better dispersion between the hydrophobic polymer and the hydrophilic clay, and to increase the interlayered spacing of the clay. The equation for calculating the intercalating agent needed for a cation-exchange reaction is

$$92.6/100 \times 10(\text{g clay}) \times 1.2 = X/M_w \text{ of intercalating agent} \times 1 \times 1000 \quad (1)$$

where X represents the amount of intercalating agent used, 92.6/100 represents the cationic exchange capacity (CEC) of 92.6 mequiv/100 g of MMT clay, and 1.2 (>1) indicates the excess amount of intercalating agent used. The intercalant, AEAPTMS (0.012 mol) and screened natural clay (10 g) were slowly added to 1000 ml of 0.01 N HCl solution and mixed well for better clay dispersion. Then the dispersion was heated to 60 °C and continuously stirred for 12 h to obtain completely ion-exchanged hydrophobic inorganic-organophilic clay. Finally the treated clay was washed with de-ionized water several times to remove residual chloride or cations. To ensure the complete removal of chloride ions, the filtrate was titrated with 0.1 N $AgNO_3$ until no further AgCl precipitated. The filter cake was then placed in a vacuum oven at 80 °C for 24 h. The dried cake was ground and screened with a 325-mesh sieve to obtain the inorganic-organophilic clay.

2.3. Synthesis of aqueous SPUA/clay nanocomposites

A 250 ml rounded, four-necked separable flask with a mechanical stirrer, nitrogen inlet, thermometer and condenser, was charged with PTMG, DMPA dissolved in NMP, BD and modified clay. The reaction was performed in a silicone oil bath maintained at a constant temperature under a nitrogen atmosphere and the mixture was agitated for 12 h at 80 °C for the exfoliation of clay by PTMG. After thorough mixing, diisocyanate (IPDI) and 0.03% DBTDL catalyst were added to the reaction mixture and the reaction was allowed to obtain NCO-terminated prepolymer for 2.5 h. Then, a calculated amount of PAPTMS was slowly added and the reaction continued for further 1.5 h. After cooling to 70 °C, MMA and MAPTMS were added to make SPUA/clay hybrid material and then TEA was added and the reaction was further continued for another 30 min. Finally, water was added with vigorous stirring to obtain uniform dispersion. The above-obtained uniform dispersion containing acrylic monomers was further polymerized with KPS solution (0.085 g in 10 ml water) by gradual addition over 30 min. The reaction was continued for 4 h to get SPUA/clay nanocomposite. The solid content of the resulting product was adjusted to 30%. The compositions for the preparation of SPUA/clay nanocomposites are given in Table 1.

The SPUA/clay nanocomposites were cast on a silicone trough and water was allowed to evaporate at room temperature. The remaining moisture was removed under a vacuum at 60 °C for 24 h. The SPUA/clay nanocomposites crosslink spontaneously through formation of silyl ether linkages upon removal of water (via a combination of hydrolysis and condensation of trimethoxysilyl groups). No additional additives or catalysts are used for crosslinking to occur.

2.4. Characterization and property measurements

The particle size of the SPUA/clay nanocomposite dispersion was measured using a BI-particle sizer ZPA (Brookhaven Inst. Co.). Fourier transform infrared (FT-IR) spectroscopy was carried out using a Bruker Tensor 27 FT-IR analyzer (Bruker Optics, Germany). Analyses were performed in the transmission mode in the range 400–4000 cm^{-1} at room temperature with a resolution of 2 cm^{-1} and accumulation of 32 scans. KBr disks were prepared after mixing (0.5%) each of the test samples with dry KBr. Wide angle X-ray diffraction (WAXD) experiments were performed directly on the film samples using an X-ray diffractometer (Rigaku D/MAX − 2500H) at 40 kV and 100 mA with a Cu Kα radiation source ($\lambda = 1.5404$ Å), at a scan speed of 4° min^{-1} and in the range of 1–30°. Nanocomposite samples were measured as films, with thicknesses of 0.1–0.3 mm.

The samples for the transmission electron microscopy (TEM, JEOL JEM3010, Japan) study were prepared by placing the SPUA/clay nanocomposite films into epoxy capsules. The capsules were cured at 70 °C for 24 h in a vacuum oven. Then, the cured epoxies containing SPUA/clay nanocomposites were microtomed into 50-nm-thick slices in a cryogenic ultra-microtome system. Subsequently, a 3-nm-thick layer of carbon was deposited onto these slices, that being on 200-mesh copper nets for TEM observation. Dynamic mechanical properties were determined using a dynamic mechanical analyzer (Seiko Exstar 6000, DMA/SS6100) with a tensile

Table 1
Composition of SPUA/clay nanocomposites (weight in grams)

Ingredient		Sample						
		C0	C1	C2	C3	A1	A2	A3
PTMG-2000		12.50	12.50	12.50	12.50	12.50	12.50	12.50
DMPA		1.41	1.41	1.41	1.41	1.41	1.41	1.41
BD		0.51	0.51	0.51	0.51	0.51	0.51	0.51
NMP		6.00	6.00	6.00	6.00	6.00	6.00	6.00
IPDI		7.00	7.00	7.00	7.00	7.00	7.00	7.00
PAPTMS		4.06	4.06	4.06	4.06	4.06	4.06	4.06
MMA		6.82	6.82	6.82	6.82	6.82	6.82	6.82
MAPTMS		1.70	1.70	1.70	1.70	1.70	1.70	1.70
TEA		1.07	1.07	1.07	1.07	1.07	1.07	1.07
Clay (%)	Cloisite 10A	0.00	1.00	2.00	3.00	–	–	–
	AEAPTMS-modified clay	–	–	–	–	1.00	2.00	3.00

Initiator: KPS 0.085 g in 10 ml water, reaction temperature 70 °C.

mode. The geometry of the specimens was 10 mm (length) × 7 mm (width) × 0.1 mm (thickness). The samples were cooled to −100 °C, equilibrated for 3 min, and then heated to 150 °C with a constant heating rate of 5 °C/min and a frequency of 1 Hz, under a nitrogen atmosphere. Tensile properties of the dispersion-cast films were measured using a universal tensile machine (INSTRON, UK) at a crosshead speed of 0.1 m min^{-1}. Sample specimens were prepared from the films with a 10 mm × 40 mm die with the grip distance set at 20 mm. The thicknesses of the films were between 0.1 mm and 0.3 mm. For each film, three specimens were tested and the average value was reported. A thermogravimetric analysis (TGA, TA Instruments, Q50, USA) was carried out and the sample weights were 3–10 mg. Experimental runs were performed from 30 to 800 °C at a heating rate of 10 °C/min in a nitrogen atmosphere, with a gas flow rate of 30 ml min^{-1}.

The gel content was calculated as follows: A sample of approximately 0.1 g (W_1) was wrapped in 300-mesh stainless steel mesh of a known mass (W_2) and exposed to 100 ml of xylene at 100 °C for 24 h. The stainless steel mesh was then removed and the mass was measured after vacuum drying at 80 °C for 24 h (W_3). The degree of crosslinking was measured in terms of the percentage of gel content, using the equation:

$$\text{Gel content}\ (\%) = (W_3 - W_2)/W_1 \times 100 \quad (2)$$

The water and xylene resistance values of the films were tested as follows: pre-weighed dry slabs (5 mm × 5 mm in size) were immersed in DI water and xylene, respectively, at 25 °C. After immersion, the samples were blotted with laboratory tissue and weighed. The swelling (solvent uptake) was expressed as the weight percentage of water in the swollen sample:

$$\text{Swelling}\ (\%) = (W_S - W_D)/W_D \times 100 \quad (3)$$

where W_D is the weight of the dry sample and W_S is the weight of the swollen sample.

3. Results and discussion

3.1. Silylation of natural clay with organo-functional trialkoxysilane

Pristine clay is hydrophilic and can form a stable dispersion in water, in which clay is dispersed as isolated sheets or small domains consisting of a few sheets [23]. A schematic illustration of silylation of pristine clay is shown in Scheme 1 and characteristics of clays are presented in Table 2. There are two purposes for modifying pristine clay by organo-functional trialkoxysilane. One is to modify the surface of clay with the alkoxy group of silane through the condensation reaction of the OH group of clay with the alkoxy group of silane; another is to replace sodium ions for a better exfoliation/dispersion of modified clay in SPUA prepolymer. This method also promotes the oligomerization of silane during surface modification, since the condensation reaction can be catalyzed by the presence of water or autocatalyzed. In contrast to most other organo-functional silanes, the hydrolysis and condensation of silanes having primary amino functions in aqueous solutions are autocatalyzed. This is evident from the pronounced polarization of the molecule (electrostatic interaction of $NH_2 \leftrightarrow SiOR$, R is alkyl group) and from the strong interaction of the NH_2 group with the polar solvent itself [24].

The changes in morphology of the clay were monitored using WAXD. The WAXD diagrams of pristine clay as well as well-dried modified clay are shown in Fig. 1. The *d*-spacing of the pristine clay was about 1.17 nm, which agrees well with many previous reports [25]. The *d*-spacing of the modified clay and Cloisite 10A were ∼1.55 nm ($2\theta = 5.7°$) and ∼1.92 nm ($2\theta = 4.6°$), respectively. The *d*-spacing difference between the pristine clay and modified clay was about 0.4 nm, and it is estimated that there may be a single molecular layer between each clay layer. The increase in the basal spacings suggests that polycondensates are formed in the interlaminate space. This is understandable because the silane preferentially replaces the sodium ions on the surface of the clay platelets with ammonium ions from the silane and these are grafted at the edge of the clay platelets due to the existence of a hydroxyl group at the edge of the clay platelets [26]. Modification with AEAPTMS did not affect the microstructure much

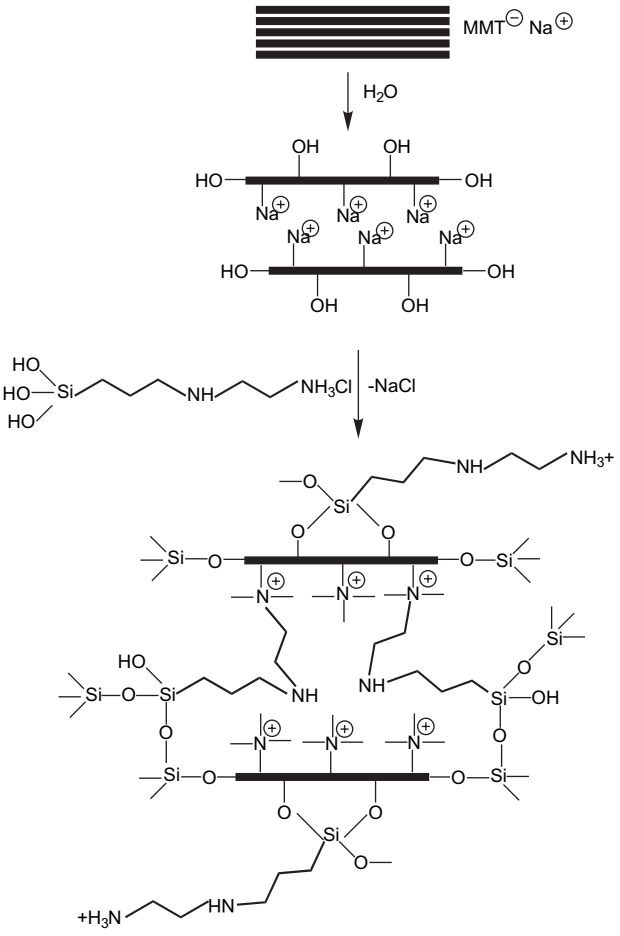

Scheme 1. Schematic illustration of silylation of pristine clay.

Table 2
Properties of pristine clay, modified clay and Cloisite 10A

Clay	Property						
	Organic modifier	Cation exchange capacity (mequiv/100 g clay)	$2\theta^{\circ}$	d_{001} (nm)	Weight loss (%)[a]	Grafted amount (mequiv/g)[b]	Grafted yield (%)[c]
Cloisite Na^{+}	None	92.6	7.2	1.17	–	–	–
AEAPTMS-clay	AEAPTMS	92.6	5.7	1.55	14.2	0.74	61.7
Cloisite 10A	2MBHT[d]	125	4.6	1.92	–	–	–

[a] Weight loss between 200 and 600 °C.
[b] Determined using Eq. (4).
[c] Determined using Eq. (5).
[d] Dimethyl, benzyl, hydrogenated tallow.

because it is a short chain oligomer. To understand our data, it must be considered that the silylation reaction produces siloxane polymers able to penetrate the external part of the interlaminate space and push the clay sheets apart [13]. It is clear that the combined reaction of ion replacement on the surface of the clay platelets and grafting at the edge of the clay platelets by a short chain, and preferentially the same modifier molecule, controls or limits the interlayer spacing of the clay sheets. However, even with such minimal modification, the resulting SPUA/clay nanocomposites exhibit an improved morphology (Scheme 1).

Thermogravimetric analysis (TGA) was performed on the materials to obtain information on their degradation. Fig. 2 provides the TGA curves of pristine clay, AEAPTMS-clay and Cloisite 10A. The multistage degradation temperatures of Cloisite 10A, as measured in a TGA at a ramp rate of 20 °C/min, were about 200 °C, 270 °C and 390 °C. The degradation, which starts at 270 °C and above, may be attributed to the release of olefin and amine [27]. The unmodified clay showed negligible decomposition up to 800 °C. In the region of 600 °C, a mass loss has been previously assigned to the loss of structural hydroxyl water from MMT. AEAPTMS-modified clay exhibits a higher onset temperature of about 310 °C, and the second decomposition step starts above 400 °C. The above-mentioned decompositions are probably due to the loss of structural hydroxyl water and organosilyl groups of modified clay. The organosilyl group is released very slowly between 400 and 500 °C and more quickly between 500 and 700 °C. Similar results have been reported [11], in that the organosilyl groups grafted to the silicates are highly thermally stable and that decomposition does not begin below 400 °C.

The grafted amount was determined using the following equation based on the weight loss, $W_{200-600}$, that is between 200 and 600 °C, corresponding to silane degradation [13].

$$\text{Grafted amount (mequiv/g)} = \left(10^3 W_{200-600}\right) / \times (100 - W_{200-600})M \qquad (4)$$

where M (g/mol) is the molecular weight of the grafted silane molecules. The grafting yield, which corresponds to the percentage of silane molecules effectively involved in the coupling reaction, was calculated as follows:

$$\text{Grafting yield (\%)} = \text{grafted amount} \times 100/[\text{silane}] \qquad (5)$$

where [silane] (mequiv/g) is the initial silane concentration. The weight loss between 200 °C and 600 °C, grafted amount and grafting yield are listed in Table 2. The weight loss

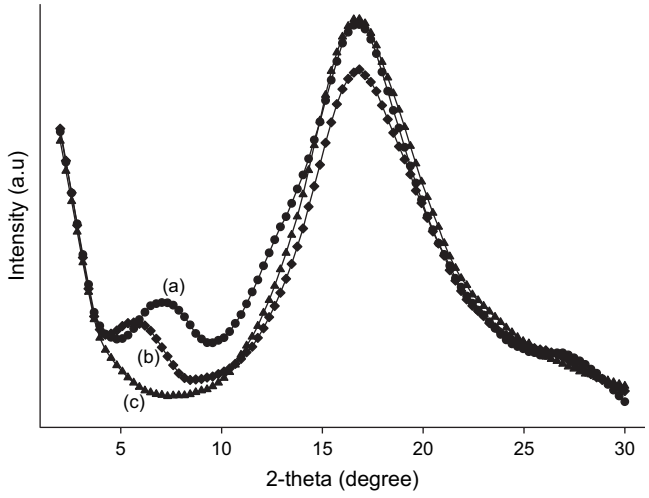

Fig. 1. XRD patterns of (a) pristine clay, (b) AEAPTMS-modified clay and (c) Cloisite 10A.

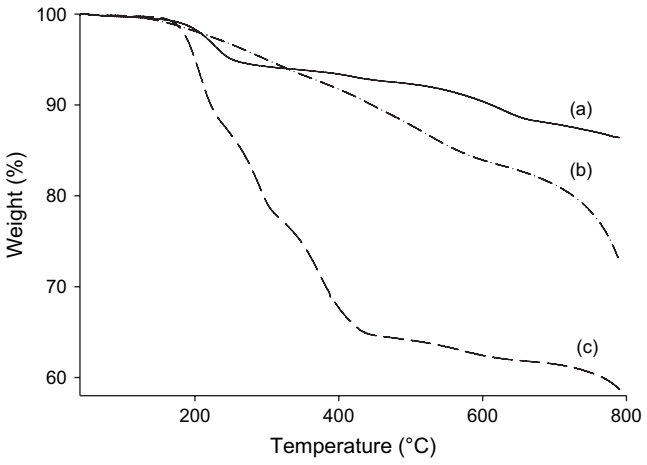

Fig. 2. TGA curves of (a) pristine clay, (b) AEAPTMS-modified clay and (c) Cloisite 10A.

between 200 °C and 600 °C was 14.2% and the grafted yield was 61.7%. The grafted amount of silane determined by TGA analysis was 0.74 mequiv/g, which was in good agreement with the cation exchange capacity (CEC, 92.6 mequiv/100 g) of the pristine clay. These results show that the cations (sodium ions) of the pristine clay are completely replaced by both primary and secondary quaternary ammonium ions of the AEAPTMS-modifier. It is assumed that 0.463 mequiv/g of AEAPTMS is required to replace all of the cations of the pristine clay (if both primary and secondary quaternary ammonium ions are involved). But the results confirm that about 20% of the secondary quaternary ammonium ions ($-CH_2-NH_2^+-CH_2-$) of AEAPTMS may be consumed for cation (Na^+) replacement (not shown in the Scheme 1). Primary quaternary ammonium ions ($-CH_2-NH_3^+$) of AEAPTMS may replace 80% of the sodium cations. It is also believed that the trifunctional AEAPTMS-modifier can form oligomers attached to the clay edges by two or three Si–OMe groups. The formation of chemical bonds between the individual clay platelets gives rise to irreversibly attached clay stacks [13]. The evidence for the reaction between the silane and clay platelets comes from FT-IR studies. Fig. 3 shows the FT-IR curves of pristine clay, AEAPTMS-clay and Cloisite 10A. The FT-IR spectrum of pristine clay displays typical –OH stretching at 3627 cm^{-1}, and broad bands at 3425 and 1635 cm^{-1} can be attributed to adsorbed water molecules [28]. The strong broad band in the region of 1000–1130 cm^{-1} is likely due to siloxane (Si–O–Si) bond. The bands at 1115, 1035, and 915 cm^{-1} can be collectively attributed to Si–O stretching vibrations [29]. The spectrum of silane-modified clay displays almost the same pattern as that of pristine clay, except for some new bands at 2935 cm^{-1} with a small hump at 2850 cm^{-1} that are due to the –CH asymmetric and symmetric stretching of $-CH_2$ groups which confirms the presence of the silane on the surface. Also, new peak at 1464 cm^{-1} that corresponds to the $-CH_2$ bending vibrations further supports this conclusion.

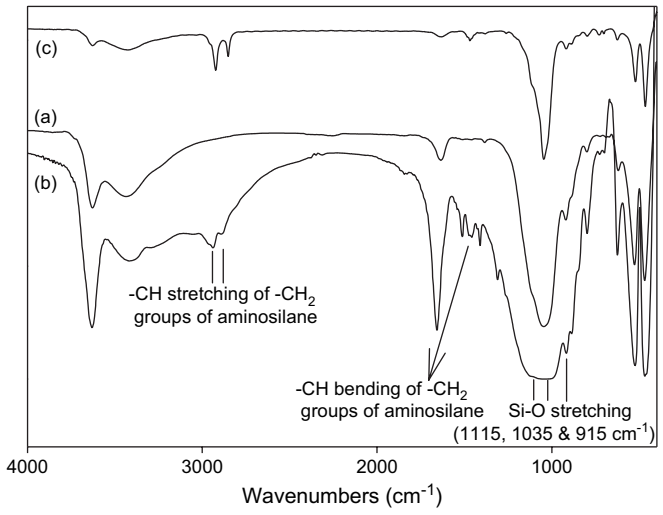

Fig. 3. FT-IR spectra of (a) pristine clay, (b) AEAPTMS-modified clay and (c) Cloisite 10A.

3.2. Synthesis of SPUA/clay nanocomposite dispersions, particle size and stability

Two series of SPUA/clay nanocomposite (Cloisite 10A-based and AEAPTMS-clay-based) dispersions were synthesized by adding 1, 2 and 3% of organoclay. The recipes are given in Table 1. Neat SPUA was also prepared and studied in order to compare the results with the SPUA/clay nanocomposites. Scheme 2 outlines the synthetic process for the preparation of SPUAs at a ratio of 1.4 NCO/OH and their dispersions. Since SPU prepolymers were highly sensitive to moisture and are more viscous than those of pure PU prepolymers, these were diluted with MMA and MAPTMS monomer mixture before dispersing the SPU prepolymers in water to avoid pre-crosslinking [21]. Here MMA and MAPTMS were used as solvents instead of other organic solvents. The DMPA content was kept at 0.021 mol in these experiments. The carboxylic groups of the DMPA were neutralized by equimolar amounts of TEA and the pHs of the dispersions were basic. The solid content of all the dispersions were checked and adjusted to 30%. All these experiments were carried out with care in a nitrogen atmosphere to avoid premature crosslinking or gellation. The SPUA/clay nanocomposite dispersions showed no precipitates or unstable aggregates.

FT-IR spectra of representative SPUA/clay nanocomposites C3, A3 and PAPTMS are given in Fig. 4. The peaks at 1700 and 1656 cm^{-1} are due to the free and ion-interacted C=O stretchings, respectively. The absorptions peaks at 2900 cm^{-1} (CH_2 stretching vibration of PTMG), 1100 cm^{-1} (C–O–C stretching vibration of PTMG, Si–O–C stretching and Si–O–Si asymmetric stretching vibration of amino silane), 3250–3300 cm^{-1} (N–H stretching), 1530–1560 cm^{-1} (N–H bending), 1210–1240 cm^{-1} (the stretching vibration of the C=O group of urea combined with the N–H group and propyl (alkyl) group of three types of silanes) and about 755–840 cm^{-1} (Si–C stretching and Si–O–C deformation) confirmed the formation of SPUA/clay nanocomposites [21].

The organoclay in the aqueous dispersions swells and its layers are separated by hydration, which provides good dispersions in the SPUA/clay nanocomposite. Generally, the particle size of the SPUA/clay nanocomposite depends mainly on the hydrophilicity, degree of neutralization, viscosity of the prepolymer, clay content, and crosslinking density. The particles' sizes of the SPUA/clay nanocomposite dispersions (30 wt% solid contents) are presented in Table 3. In these two series, the particle size of the dispersions was between 25 and 40 nm. This marginal difference could be due to the presence of the same molar level of the neutralized DMPA in all dispersions and the dispersion of NCO-free SPUA prepolymer in water. Another reason for the marginal increase in average particle diameter with the increase in clay content could be the better dispersion and the hydrophobic nature of organosilyl groups of the modified clay. This increase could also possibly result from the ionic interactions between SPUA and clay. The SPUA dispersion is electrostatically stabilized by $-COO^-$ ions of neutralized DMPA. Therefore, a stable electrical double layer is formed around each SPUA particle. The cations of

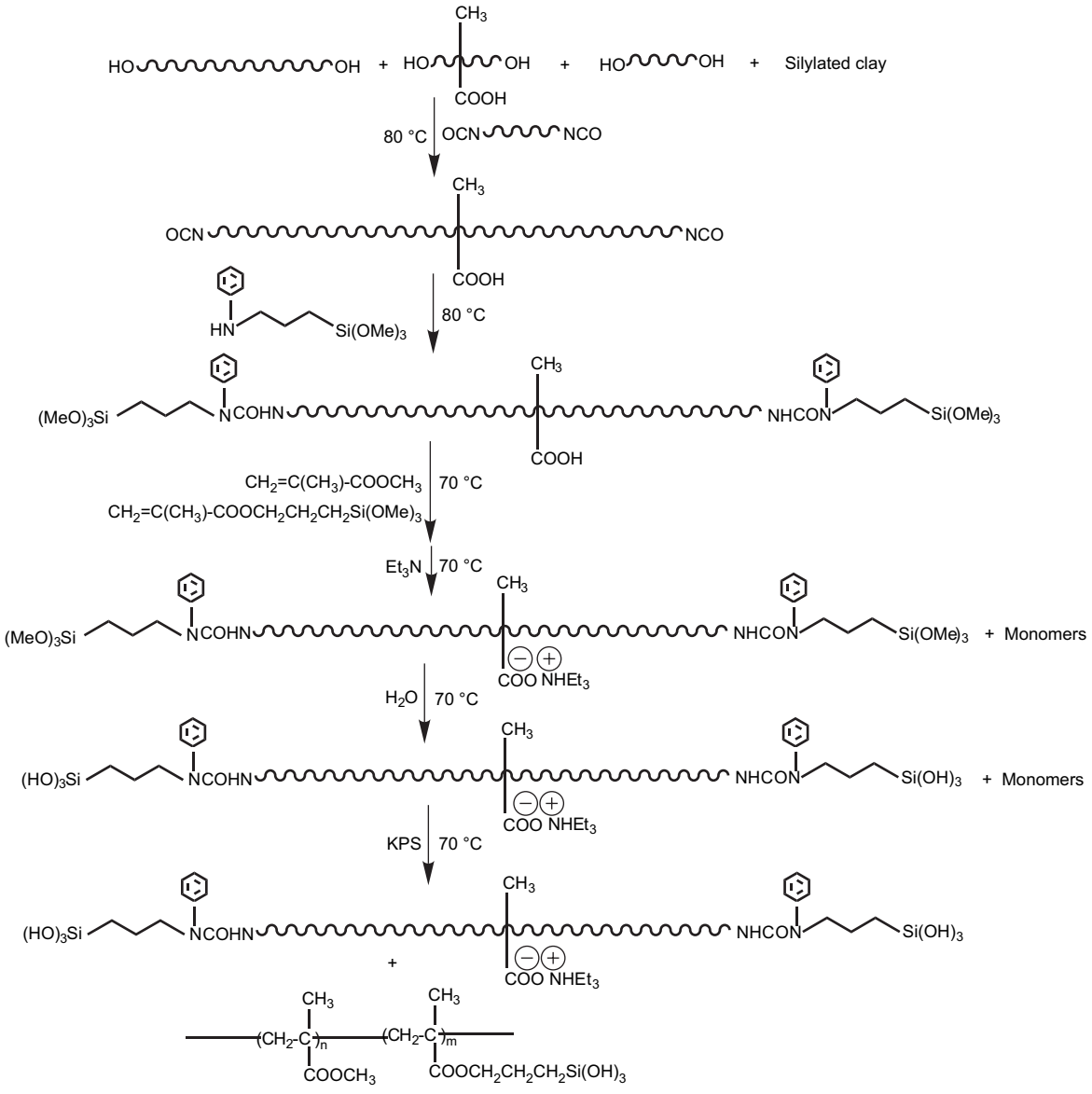

Scheme 2. Synthetic scheme of SPUA/clay nanocomposite.

exfoliated clay platelets interact with $-COO^-$ ions and interfere with the double layer of neat SPUA dispersion. In the self-emulsification of ionomers, particle size increases with a decrease in hydrophilicity, which is governed by the ionic content of PU prepolymers [22]. In these experiments, the content of organoclay is another variable in both sets of dispersions, and the variations showed that clay has a marginal effect on the particle size. This result shows that the clay particles were well dispersed in the SPUA polymer matrix, without any agglomeration probably because of the hydrophobic nature of both the modified clay surface and the matrix. Since the isocyanate (NCO) groups were completely end-capped with PAPTMS and compatible with silylated acrylic polymer, there were no side reactions or precipitation in the resulting dispersion [21]. The SPUAs and their nanocomposites, which were stored at room temperature for 12 months, were also stable.

3.3. Morphology of SPUA/clay nanocomposite films

WAXD is the most powerful technique for monitoring the formation and structure of intercalated or exfoliated organoclays. WAXD patterns of the nanocomposite films are shown in Fig. 5(A) and (B). It can be seen from the WAXD pictures that there is no distinguishable peak in the SPUA/clay nanocomposite films of C1, C2, C3, A1, and A2 in the range of $2\theta = 1-12^\circ$. This shows that the *d*-spacing increases when SPUA is combined with the clay, probably because the SPUA penetrates into the gallery space and forces the galleries apart. There is more chance for SPUA chains to intercalate or

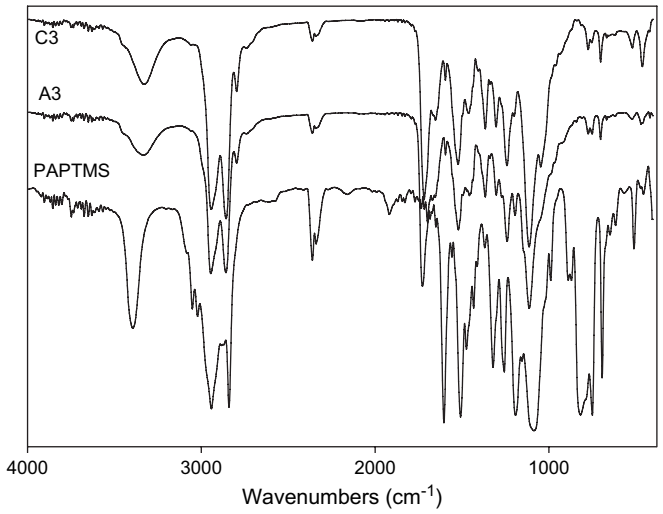

Fig. 4. FT-IR spectra of (a) PAPTMS, (b) A3 and (c) C3.

exfoliate into the gallery with AEAPTMS-silicate and Closite 10A having less silicate in the nanocomposite [30]. After modification of neat clay by AEAPTMS, the wetting ability between the SPUA and the modified clay was improved because the surface OH groups at the edges of the layers have been lost and this leads to the better intercalation or exfoliation process. On the other hand, a weak peak was observed in the WAXD patterns of A3, when the organophilic clay content was 3.0%. The peaks ($2\theta = 5.2^\circ$) may have occurred because the content of organoclay increases in the nanocomposite. This indicates that the silicate layers of organoclays dispersed in the SPUA matrix lose their structural registry due to intercalation. This result also suggests that the layered silicates in the SPUA/clay nanocomposites (A3) might be mostly intercalated in the SPUA matrix [21,31]. It has been reported that the complete and effective entry of the PU molecules into the organic modified silicate layers, that caused a thorough exfoliation of the silicate layers in the SPU matrix, could not be achieved with a higher content of organoclay [21]. The intercalation of AEAPTMS-based clay nanocomposites may also be due to low *d*-spacing value and chemical linkages formed between individual clay platelets. For many solvent-based PU/clay nanocomposites with an absence of ions in PU moieties, the electrostatic forces between the clay platelets would

Table 3
Tensile properties and particle size of SPUA/clay nanocomposites

Sample	Property		
	Tensile strength (MPa)	Elongation (%)	Particle size (nm)
C0	9.1	50	27.2
C1	15.2	304	26.4
C2	11.1	173	28.1
C3	12.9	217	30.2
A1	16.2	11	26.9
A2	15.8	30	31.2
A3	20.3	23	35.5

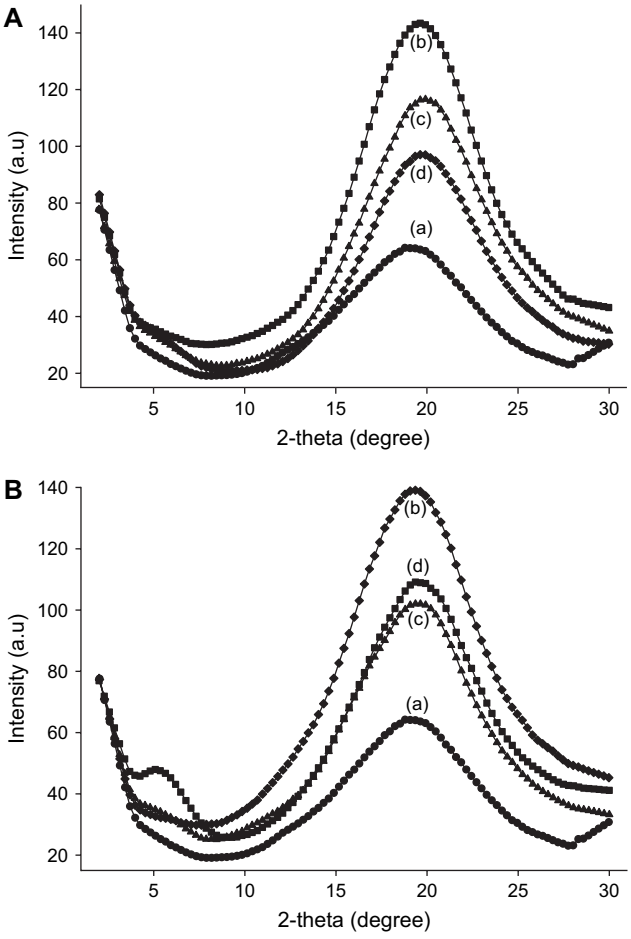

Fig. 5. (A) XRD patterns of (a) C0, (b) C1, (c) C2 and (d) C3 SPUA/clay nanocomposite films. (B) XRD patterns of (a) C0, (b) A1, (c) A2 and (d) A3 SPUA/clay nanocomposite films.

have a tendency to squeeze the PU polymer chains out and subsequently result in an intercalated structure [31,32]. For a certain SPUA/clay nanocomposite, the above-mentioned squeeze effect was overcome by the ionic attractions between anionic SPUAs and cationic clay platelets [22], resulting in an exfoliated silicate system.

Conventional TEM can directly provide more information in real space, in a localized area, and on morphology and defect structures. Since it is difficult to draw definitive conclusions about the structure of hybrids from the WAXD patterns, TEM is necessary for determining the nature of the hybrids. In addition, it provides additional information that will aid in the interpretation of the WAXD results. Typical TEM images of SPUA/clay nanocomposites of samples C1, C3, A1 and A3 are shown in Fig. 6(a)–(d), and these can be observed with the presence of one or several clay layers in the SPUA matrix, which indicates the dispersion of clay layers in the SPUA matrix and the formation of nanocomposites. TEM micrographs also prove that most clay layers are dispersed homogeneously into the polymer matrix. The dark lines in the micrographs represent the clay layers, and the spaces between the dark lines are interlayer spaces. Some single

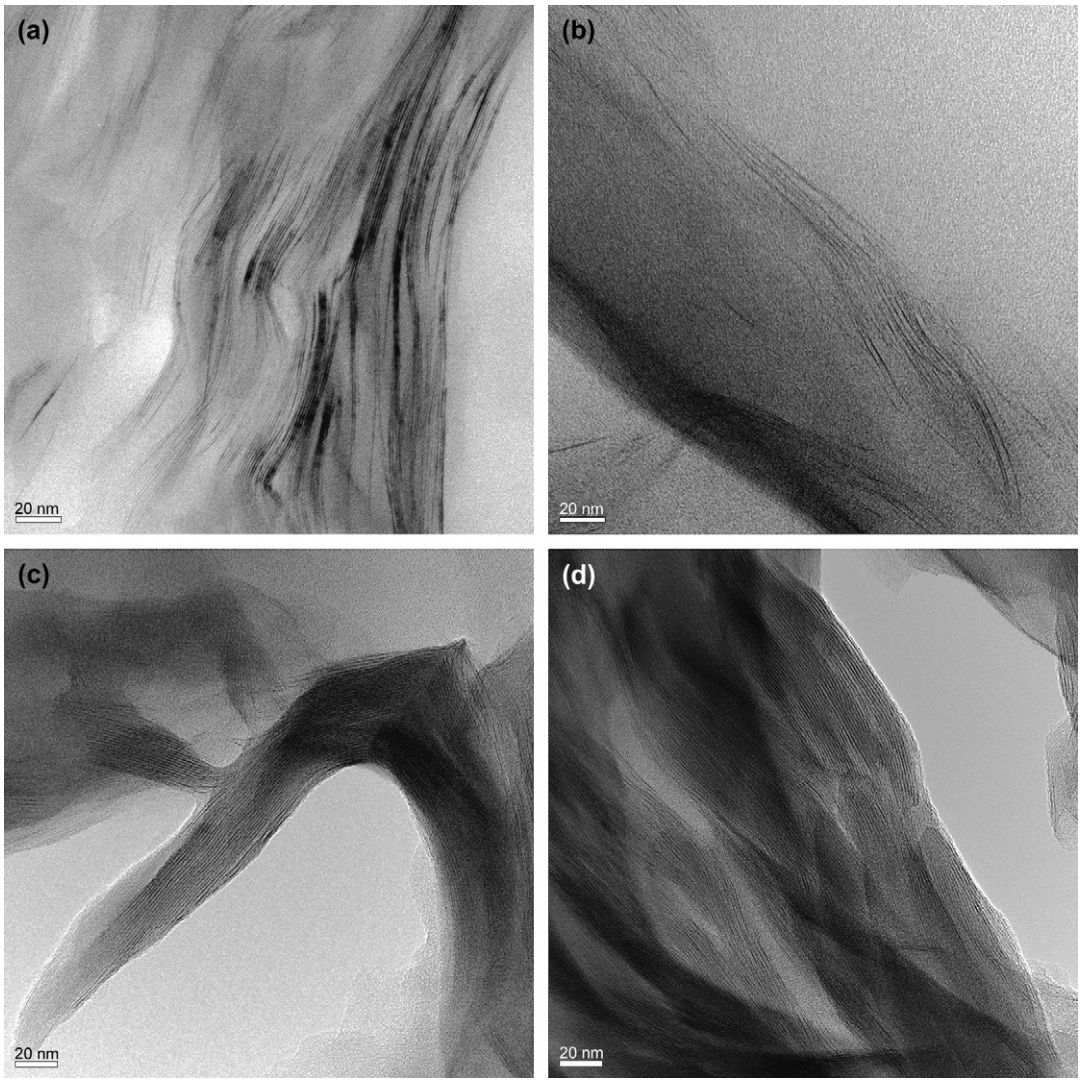

Fig. 6. TEM images of (a) C1, (b) C3, (c) A1 and (d) A3 SPUA/clay nanocomposite films.

silicate layers and ordered intercalated or exfoliated assembled layers of clay are well dispersed in the SPUA matrix. Fig. 6 shows a higher magnification revealing that organoclay is mostly intercalated or partially exfoliated in the SPUA matrix with layer distances of 2–3 nm. The dark lines are the cross-sections of single or possibly multiple-silicate platelets. The platelets are flexible and, thus, show some curvature. This result confirmed that the layered silicates were mostly intercalated or partially exfoliated in the SPUA/clay nanocomposites, and the individual silicate layers have much less separation between them. On the basis of the aforementioned TEM and WAXD results, the SPUA/clay dispersion sample was apparently a nanocomposite with mostly intercalated or partially exfoliated structures of organoclay [21,31]. The combined effect of the decrease in interlayer attraction and the improvement in the wetting ability promote the intercalation of SPUA into interlayers. It is worth mentioning that the study of AEAPTMS-clay in neat SPUA will provide more basic information on the dispersion mechanism of clay in the polymer matrix compared to aqueous SPUA/clay nanocomposite.

3.4. Tensile properties of SPUA/clay nanocomposite films

Mechanical properties were tested and compared to study the efficiency of surface modification to obtain a supportive evidence of the enhanced intercalation of clay. As shown in Table 3, silylation of pristine clays imparts a change of the tensile strength to the nanocomposite materials. It was clear from the test results that both the tensile strength and the elongations at break increase as the organoclay content increases in Cloisite 10A-based SPUA/clay nanocomposites. Unlike Cloisite 10A-based SPUA/clay nanocomposites, the tensile strength increases and the elongations at break decrease with an increase in the organoclay content in AEAPTMS-based SPUA/clay nanocomposites. These results imply that the greater dissociation of clay silicate layers and their homogeneous distribution in the polymer matrix was well established by surface modification of the clay. Between the two series of the nanocomposites, AEAPTMS-based SPUA/clay nanocomposite films exhibit higher tensile properties compared to the

commercial Cloisite 10A-based SPUA/clay nanocomposite. Swelled clay can be regarded as a crosslinking center of SPUA polymer via an AEAPTMS-modifier, consequently promoting the tensile strength and decreasing the elongation of the nanocomposites. The tensile strength of AEAPTMS-based SPUA/clay nanocomposite is about 30–40% higher than that of the Cloisite 10A-based SPUA/clay nanocomposites. The elongation at break of the Cloisite 10A-based SPUA/clay nanocomposites is several times higher than that of the AEAPTMS-based SPUA/clay nanocomposite. This result confirms that the combined silylation effect of three materials, silylated clay, silylated PU and silylated acrylic make the resultant nanocomposite a highly crosslinked tough material. There are several other explanations responsible for the improvement in mechanical properties such as (i) ionic interactions between the SPUA and silylated clay may strengthen the SPUA by reducing slippage during straining, (ii) the clay may act as nucleation sites to promote soft-segment crystallization during straining, (iii) the clay may act as physical entanglements to reinforce tensile properties of the composites, and (iv) the clay may alter the strained microphase morphology of the SPUA in such a way that results in improved tensile properties [32]. The improvement in the tensile strength of the nanocomposites indicated that there is a strong interfacial interaction between the modified clay surface and the nearby silylated polymer chains [33].

3.5. Fracture morphology of SPUA/clay nanocomposite films by SEM

Images shown in Fig. 7 are ambient fractographs of the neat SPUA and the nanocomposites. As shown in Fig. 7, the surface fracture of neat SPUA polymer is much flatter and smoother, which is clearly due to quick or brittle failure and the presence of acrylic hard polymer. Another reason for the smooth fracture surface for SPUA is that the soft phase is energetically favored [34] so that this phase will automatically rearrange to cover the fracture surface driven by the surface

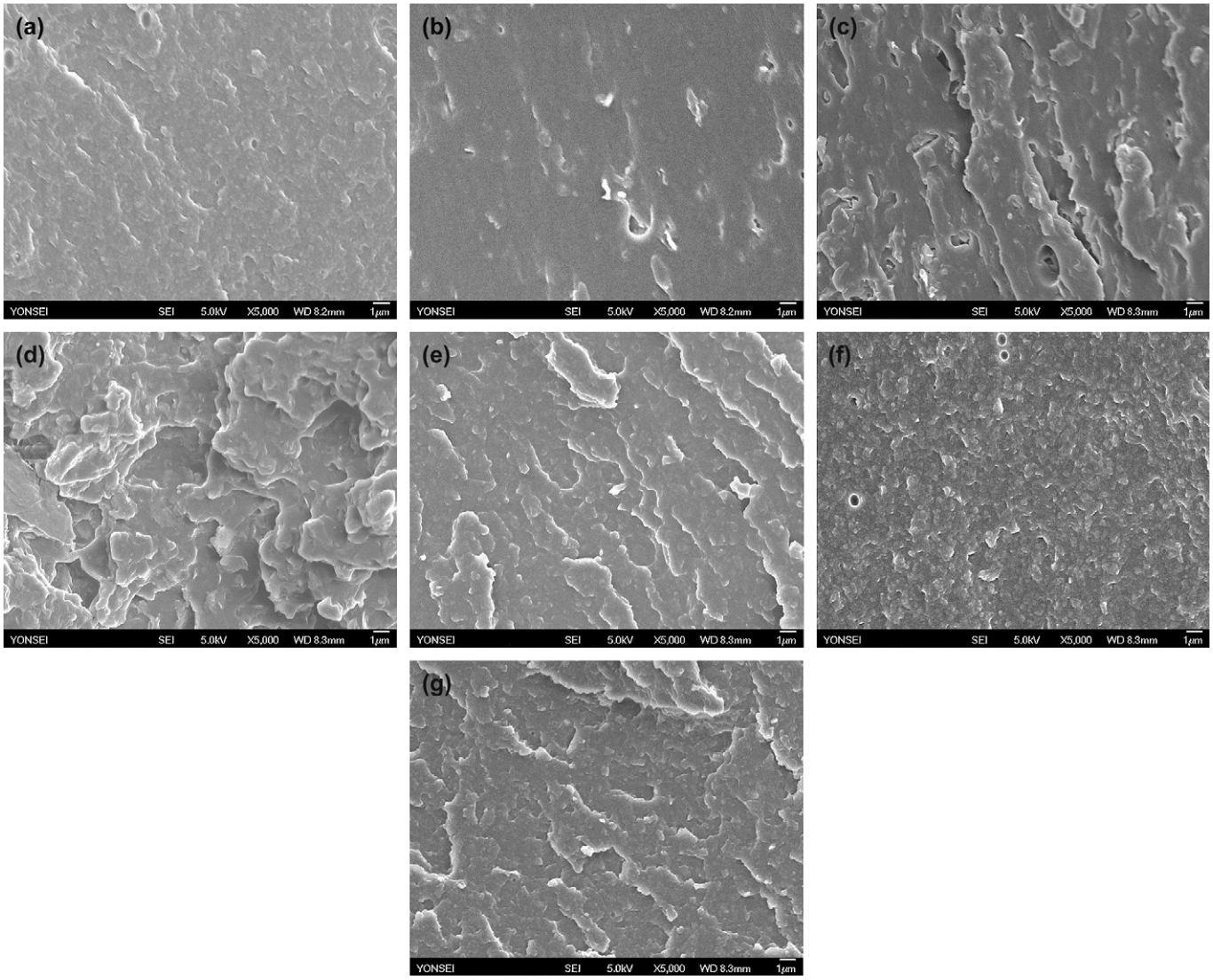

Fig. 7. SEM images of fractured surface of (a) C0, (b) C1, (c) C2, (d) C3, (e) A1, (f) A2 and (g) A3 SPUA/clay nanocomposite films.

energy. However, on addition of clay particles, the crack surface becomes rough. The roughness increases as clay content increases in the matrix. The fracture roughness indicates that the resistance of propagation of the crack is large and the crack has not propagated as easily it does in neat SPUA. The fracture surface roughness indicates that crack propagation is large and increased the torturous path of propagating crack [35]. This effect results in higher stress to failure and causes the improved strength of nanocomposites. The fracture surface of AEAPTMS-based SPUA/clay nanocomposites became rougher with large crack than Cloisite 10A-based SPUA/clay nanocomposites. The rough fracture surface of the nanocomposites results from smaller phase separation, and the special interaction between the nanoparticles and the polymer constrains the polymer chains' mobility and the efficiency of the rearrangement.

3.6. Dynamic mechanical property of SPUA/clay nanocomposite films

Fig. 8 shows the storage moduli (E') and tan δ of the nanocomposite films. The storage modulus, E', and tan δ of AEAPTMS-modified clay nanocomposites are compared with those of the neat SPUA and commercial clay nanocomposites. The AEAPTMS-modified clay nanocomposites have higher E' values than those of neat SPU over the whole temperature range and E' of nanocomposites increases with an increase in the content of organoclay (Fig. 8(a)). Adding the same content of clay (1 wt%), E' of A1 was higher than those of C1 and the values of both A1 and C1 are also higher than that of neat SPUA. This may have been due to the increase in the polarity of AEAPTMS-modified clay, which enhanced its compatibility with the SPUA. The improvement in the storage modulus with less clay loading may have resulted from the strong interaction between the organoclay and the polymer matrix [21].

Fig. 8(b) and (c) depicts two damping (transition) peaks for the SPUA/clay nanocomposites. The peaks are ascribed to the glass transition temperature of the soft and hard segments of the nanocomposites. The T_g peak positions vary slightly in the nanocomposite films of both cases. The dominant peaks around 100 °C and 113 °C represent the glass transition of the hard-segment portion of commercial Cloisite 10A-based and AEAPTMS-based SPUA/clay nanocomposites, respectively. The weak broad peaks around −70 °C were the glass transition temperature of the soft-segment portion of the SPUA/clay nanocomposites. The glass transition temperature of both hard and soft-segment portions of the SPUA/clay nanocomposites had a marginal or no effect with addition of a small part by wt% of clay, because of the interaction between the SPUA polymer and clay. However, adding AEAPTMS-clay in SPUA, it appears that the AEAPTMS fraction led to an

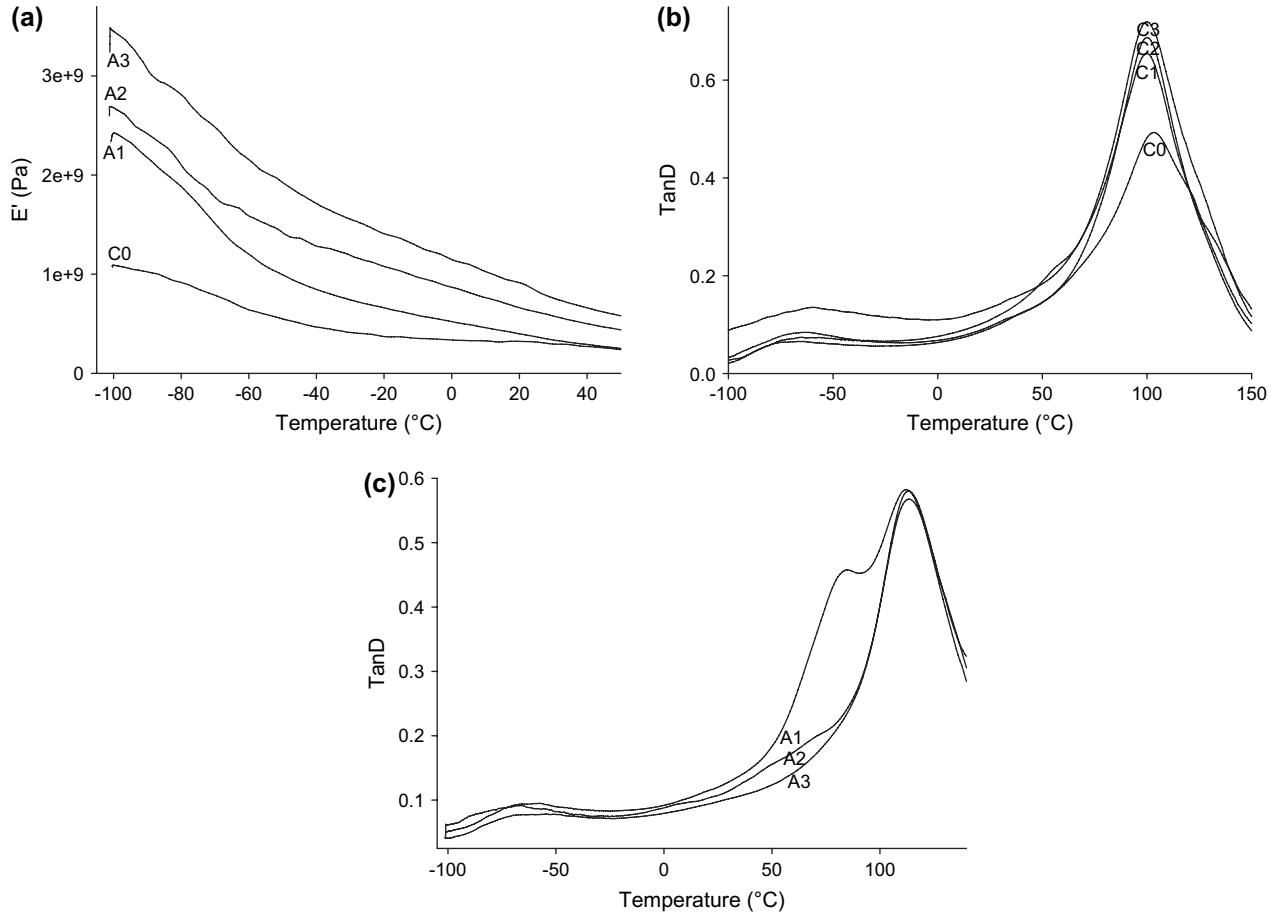

Fig. 8. (a) Storage modulus of AEAPTMS-modified clay-based SPUA/clay nanocomposite films. (b) and (c) Tan δ of the SPUA/clay nanocomposite films.

increase in the T_g of the hard segment of AEAPTMS-based SPUA/clay nanocomposites. It is more desirable to study further to understand the effect of AEAPTMS-modified clay in SPUA/clay nanocomposites, especially in non-aqueous SPUA/clay nanocomposites.

3.7. Thermal property of SPUA/clay nanocomposite films

It is generally believed that the introduction of inorganic components into organic materials can improve their thermal stability because these species posses good thermal stability [36]. The TGA curves of the neat SPUA and the SPUA/clay nanocomposites are shown in Fig. 9 and weight percentages at 350 °C are summarized in Table 4. The onset decomposition temperature (T_{OD}) of the nanocomposites and the neat SPUA are somewhat different, but this difference is not remarkable. However, the maximum decomposition temperature (T_{max}) and the weight percentages at 350 °C of the nanocomposites were remarkably higher than those of neat SPUA. It is clear from the weight percentages of the nanocomposites at 350 °C that the thermal stability of AEAPTMS-clay nanocomposites improved evidently compared to commercial Cloisite 10A-based nanocomposites. The increase in thermal stability could also be attributed to the high thermal stability of clay and the interaction between the clay particles and the polymer matrix. Also, the siloxane (−Si−O−Si−) network is formed from the methoxysilane hydrolysis−condensation reaction. In addition, thermal resistance increases with an increase in clay content. The introduction of inorganic components into organic materials can enhance their thermal resistance, as the dispersed silicate layers hinder the permeability of volatile degradation products out of the material [37,38].

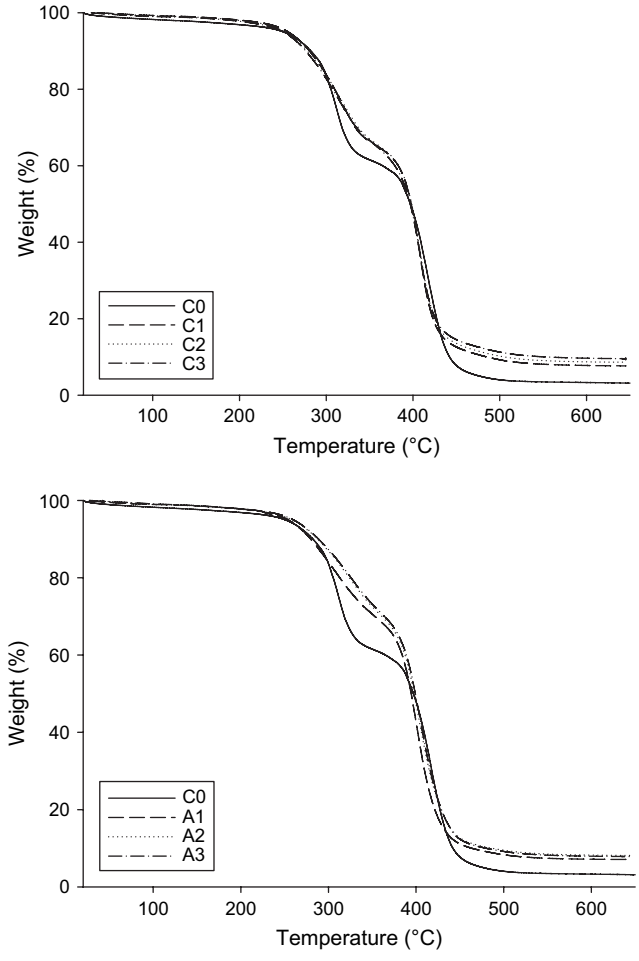

Fig. 9. TGA thermograms of the SPUA/clay nanocomposite films.

Table 4
Water and solvent swelling and gel content percentages of SPUA/clay nanocomposites

Sample	Property			
	Water swell (%) after 3 days	Xylene swell (%) in 24 h	Gel content (%)	Percentage weight at 350 °C by TGA
C0	6.7	129.5	70.8	61.5
C1	5.9	126.3	65.0	66.3
C2	4.6	121.1	68.8	67.0
C3	3.8	120.8	66.7	66.6
A1	1.8	115.4	80.5	72.4
A2	1.0	100.0	81.2	70.5
A3	0.8	93.8	82.1	73.1

3.8. Swelling of SPUA/clay nanocomposite films in water and xylene and gel content

Water and xylene resistance and gel content of the nanocomposite films were tested and are listed in Table 4. The swelling percentages of films containing 1, 2 and 3% clay were lower than those of neat SPUA film containing 0% clay and decreased with an increase in clay content. The water and xylene resistance and gel content of the AEAPTMS-clay-based nanocomposite films were remarkably superior to the commercial clay-based nanocomposite films. The presence of dispersed impermeable silicate layers in the SPUA matrix reduced water/solvent swelling and increased water/solvent resistance [21]. Improvements in water and xylene resistance of nanocomposites could be due to the intercalation of organoclay and the hydrophobicity of the treated clay. It is well known that polysiloxane have good water repellency and solvent resistance properties. Water and xylene resistance are important properties for many applications in coatings and films, especially for the water-based polymer systems.

4. Conclusions

Novel aqueous SPUA/clay nanocomposites were prepared by incorporating the organosilane-modified organophilic clay by prepolymer mixing process. The grafted amount of silane determined by thermogravimetric analysis was in good agreement (0.74 mequiv/g) with the cation exchange capacity of pristine clay. The percentage of grafting was 61.7%. This result showed that the sodium ions of pristine clay were completely replaced by both primary and secondary quaternary ammonium ions of AEAPTMS, which was grafted onto the

clay edges. X-ray diffraction and transmission electron microscopy examinations indicated that the clay platelets are mostly intercalated or partially exfoliated in the SPUA matrix. Clay does not influence the location and peak broadness of the T_g of soft segment as well as hard segment domains in the SPUA/clay nanocomposite films. But the T_g of hard segment domains was 113 °C for AEAPTMS-clay nanocomposites whereas it was 100 °C for the commercial clay-based nanocomposite. The tensile and thermal properties of silane-modified nanocomposites were superior than those of commercial clay incorporated nanocomposites. The silane-modified clay nanocomposites show higher water and xylene resistance compared to neat SPUA and the commercial clay-based nanocomposites. The most significant feature of the technique is that a very small amount of silane modifier is required to facilitate the well dispersion of the clay, which leads to better physical, mechanical and thermal properties of the resulting nanocomposites. This study effectively describes a way to prepare one-part SPUA/clay nanocomposites which have remarkable storage stability.

Acknowledgements

This work is financially supported by the Ministry of Education and Human Resources Development (MOE), the Ministry of Commerce, Industry and Energy (MOCIE) and the Ministry of Labor (MOLAB) through the fostering project of the Lab of Excellency. We also gratefully acknowledge the research funding by the Korea Institute of Industrial Technology Evaluation and Planning (Project number 10016568).

References

[1] LeBaron PC, Wang Z, Pinnavaia TJ. Appl Clay Sci 1999;15:11–29.
[2] Plueddemann EP. Silane coupling agents. New York: Plenum Press; 1982.
[3] Plueddemann EP. In: Ishida H, Kumar J, editors. Molecular characterization of composite interfaces. New York: Plenum Press; 1985. p. 13.
[4] Kim J-T, Lee D-Y, Oh T-S. J Appl Polym Sci 2003;89:2633.
[5] Hwang JJ, Liu HJ. Macromolecules 2002;35:7314–9.
[6] Subramani S, Lee JM, Kim JH, Cheong IW. Macromol Res 2005; 13:418–26.
[7] Kim BK, Seo JW, Jeong HM. Eur Polym J 2003;39:85–91.
[8] Chen T-K, Tien Y-I, Wei K-H. Polymer 2000;41:1345–53.
[9] Yanagisawa T, Kuroda K, Kato C. Bull Chem Soc Jpn 1988;61: 3743–5.
[10] Ogawa M, Okutomo S, Kuroda K. J Am Chem Soc 1998;120:7361–2.
[11] Ogawa M, Miyoshi M, Kuroda K. Chem Mater 1998;10:3787–9.
[12] Lee S, Kim J. J Polym Sci Part B Polym Phys 2004;42:2367–72.
[13] Herrera NN, Letoffe J-M, Putaux J-L, David L, Elodie B-L. Langmuir 2004;20:1564–71.
[14] Oertel G, editor. Polyurethane handbook. 3rd ed., vol. 7. Munich: Hanser Publishers; 1993.
[15] Gorrasi G, Tortora M, Vittoria V. J Polym Sci Part B Polym Phys 2005;43:2454–67.
[16] Kim DS, Kim JT, Woo WB. J Appl Polym Sci 2005;96:164–1647.
[17] Solarski S, Benali S, Rochery M, Devaux E, Alexandre M, Monteverde F, et al. J Appl Polym Sci 2005;95:238–44.
[18] Goda H, Frank CW. Chem Mater 2001;13:2783–7.
[19] Tortora M, Gorrasi G, Vittoria V, Galli G, Ritrovati S, Chiellini E. Polymer 2002;43:6147–57.
[20] Ma J, Zhang S, Qi Z. J Appl Polym Sci 2001;82:1444–8.
[21] Subramani S, Lee J-Y, Cheong IW, Kim JH. Comp Sci Technol 2007;67:1561–73.
[22] Lee H-T, Lin L-H. Macromolecules 2006;39:6133–41.
[23] Hensen EJM, Smit B. J Phys Chem 2002;B106:12664–7.
[24] Beari F, Brand M, Jenkner P, Lehnert R, Metternich HJ, Monkiewicz J, et al. J Organomet Chem 2001;625:208–16.
[25] Joseph HK. In: Kenneth PM, editor. Polymer nanocomposites. McGraw-Hill nanoscience and technology series. New York: McGraw-Hill Companies, Inc; 2006. p. 17.
[26] Carrado KA, Xu L, Csencsits R, Muntean JV. Chem Mater 2001; 13:3766–73.
[27] Zu J, Morgan AB, Lamelas FJ, Wilkie CA. Chem Mater 2001;13:3774–80.
[28] Katti DR, Katti KS, Shanmugasundaram V. Mater Res Soc Symp Proc 2002;704:257–62.
[29] Wypych F, Schreiner WH, Mattoso N, Mosca DH, Marangoni R, da Bento CAS. J Mater Chem 2003;13:304–7.
[30] Becker O, Varley R, Simon G. Polymer 2002;43:4365–73.
[31] Tien YI, Wei KH. Macromolecules 2001;34:9045–52.
[32] Finnigan B, Jack K, Campbell K, Halley P, Truss R, Casey P, et al. Macromolecules 2005;38:7386–96.
[33] Moon S-Y, Kim J-K, Nah C, Lee Y-S. Eur Polym J 2004;40:1615–21.
[34] McLean RS, Sauer BB. Macromolecules 1997;30:8314.
[35] Wu CL, Zhang MQ, Rong MZ, Friedrich K. Comp Sci Technol 2002;62:1327.
[36] Wen J, Wikes GL. Chem Mater 1996;8:1667–81.
[37] Chang J-H, An YU. J Polym Sci Part B Polym Phys 2002;40:670–7.
[38] Agag T, Koga T, Takeichi T. Polymer 2001;42:3399–408.